Allotropic phase transformation of pure zirconium by high-pressure torsion

Edalati, Kaveh
Department of Materials Science and Engineering, Faculty of Engineering, Kyushu University

Horita, Zenji
Department of Materials Science and Engineering, Faculty of Engineering, Kyushu University

Yagi, Shunsuke
Department of Materials Science and Engineering, Faculty of Engineering, Kyoto University

Matsubara, Eiichiro
Department of Materials Science and Engineering, Faculty of Engineering, Kyoto University

出版情報：Materials Science and Engineering : A. 523 (1/2), pp.277-281, 2009-10-15. Elsevier
バージョン：

Materials Science and Engineering A 523 (2009) 277–281

Received 28 December 2008; Received in revised from 29 May 2009; Accepted 16 July 2009

Allotropic phase transformation of pure zirconium by high-pressure torsion

Kaveh Edalati[a,*], Zenji Horita[a], Shunsuke Yagi[b], Eiichiro Matsubara[b]

[a] Department of Materials Science and Engineering, Faculty of Engineering, Kyushu University, Fukuoka 819-0395, Japan

[b] Department of Materials Science and Engineering, Faculty of Engineering, Kyoto University, Kyoto 606-8501, Japan

Abstract

Pure Zr is processed by high-pressure torsion (HPT) at pressures in the range of 1-40 GPa. A phase transformation occurs from α to ω phase during HPT at pressures above ~4 GPa while the total fraction of ω phase increases with straining and saturates to a constant level at higher strain. This phase transformation leads to microstructural refinement, hardness and strength enhancement and ductility reduction. Lattice parameter measurements confirm that c for α phase is expanded about 0.6% by the presence of ω phase. The temperature for reverse transformation from ω to α phase increases with straining and thus, straining under high pressure increases thermal stability of ω phase. The ω phase obtained by HPT is stable for more than 400 days at room temperature.

Keywords: Zirconium; High-pressure torsion; Severe plastic deformation; Omega phase; Phase transformation; Allotropic transformation.

* Corresponding author. Tel.: +81 92 802 2992; fax: +81 92 802 2992.

E-mail address: kaveh.edalati@zaiko6.zaiko.kyushu-u.ac.jp (K. Edalati).

1. Introduction

To achieve ultrafine-grained (UFG) materials with high strength and reasonable ductility, a great attention has been allocated to the application of severe plastic deformation (SPD) [1–3]. Despite the numerous researches for SPD processing of different pure metals, there are limited reports for pure Zr [4–12]. Coarse-grained Zr is widely used as a material for fuel cells in nuclear power plants. Recently Saldana et al. [8] developed a new application of UFG Zr as a promising biomaterial for surgical implants because of its good mechanical properties and excellent *in vitro* biocompatibility.

Pure Zr, as similar to pure Ti, can transform froman α phase with the *hcp* crystal structure to an ω phase with the simple hexagonal structure at pressures higher than 2 GPa [13–16]. Zilbershtein et al. [17] found that shear straining under pressure is very effective to induce the α→ω phase transformations in Ti and Zr. A recent study showed that a bulk form of UFG Zr was produced by application of high-pressure torsion (HPT) with the formation of an ω-phase structure [10]. There are some systematic reports regarding the effect of shear strain on the fraction of ω phase in Ti such that the fraction of ω phase increases with increasing the strain [18,19]. However, for Zr there is limited information about the role of strain on the α→ω phase transformations [10,17] and little is understood regarding the influence of pressure and shear strain on the temperature of this phase transformation as well as on the mechanical properties of HPT-processed Zr.

In this study, thus, pure Zr is processed by HPT over a wide range of strain under various pressures up to 40 GPa. The Vickers microhardness and tensile properties are investigated together with microstructural evolution including phase transformation.

2. Experimental materials and procedures

Cylindrical rods of pure Zr (99.9%) with 10mm diameter and 10mm length having impurities of 0.02% Al, 0.01% Cr and 0.07% Fe, in weight percent, were used in this study. The rods were annealed for 1h at 800 ^{o}C under an argon atmosphere and sliced to discs with thickness of 0.8 mm and diameters of 4 and 10 mm using a wire-cutting electric discharge machine. HPT was conducted at room temperature on the annealed discs using the facility as schematically illustrated in Fig. 1(a). Two sets of upper and lower anvils with a circular flat-bottom hole at the center were used to process the disc samples. The hole depths were 0.25 and the hole diameters were 4 or 10mm, respectively, with a nitrified surface with the roughness of ~30 μm. The surface profile for holes obtained by scanning laser microscopy is shown in Fig. 1(b). The disc samples with 10mm diameters were processed to N = 10 revolutions under a selected pressure in the range of 1.2–4 GPa and to N = 0, 1/4, 1/2, 1, 2, 4, 10 and 20 revolutions under a pressure of 6 GPa. The disc samples with 4mm diameter were processed to N = 5 revolutions at pressures in the range of 14–40 GPa. The rotation speed was 0.2 rpm for both 4 and 10mm diameter discs. It should be noted that the pressure was calculated by dividing the applied load by the area of the central hole on the anvil. Nevertheless, the pressure was not rigorously evaluated in this study because of the difficulty in direct measurement under very restricted condition so that it should be taken as the nominal pressure in this study. The equivalent strain was calculated by the equation as [20]:

$$\varepsilon = (1-s)\int_0^N \frac{2\pi r}{\sqrt{3}\, t(N)} dN \qquad (1)$$

where r is the distance from the center of disc, N is the number of revolutions, s is the fraction of sample slippage and $t(N)$ is the thickness of disc as a function of N determined by fitting of experimentally measured thicknesses. In this study, the fraction of slippage was 0.06 and 0.12 for the applied pressures of 2 and 6 GPa, respectively. Both fractions were independent of the number of revolutions in consistence with an earlier report [21].

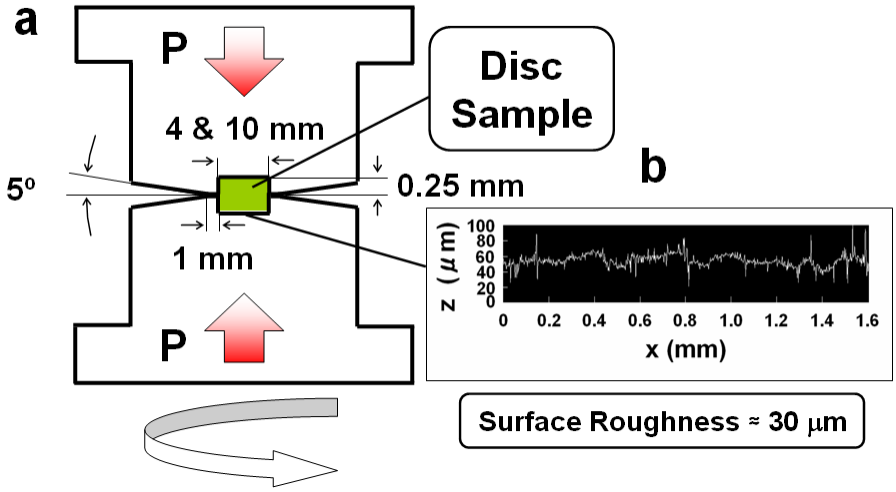

Fig. 1. (a) Schematic illustration of HPT facility and (b) surface profile of central shallow hole.

Measurements of Vickers microhardness were carried out for the HPT-processed discs with 4 and 10mm diameters. The discs with 10mm diameter were further examined by tensile testing, transmission electron microscopy (TEM), X-ray diffraction (XRD) analysis and differential scanning calorimetry (DSC). After processing by HPT, disc samples were first polished to a mirror-like surface and the Vickers microhardness was measured with an applied load of 200 g for 15 s at 8 different positions located 1.5 and 2mm distances from the center for the 4 and 10mm diameter discs, respectively. Thereafter, miniature tensile specimens having 1.5mm gauge length, 0.7mm width and 0.5mm thickness were cut from the discs at 2mmaway from the center using the wire-cutting electric discharge machining. Each tensile specimen was mounted horizontally on grips and pulled to failure at room temperature with an initial strain rate of 1.5×10^{-3} s^{-1}. For XRD analysis, discs with 3mm diameter were punched out from the HPT discs at 3.5 mm away from the center. The 3mm discs were ground and polished mechanically to a thickness of 0.5 mm and X-ray structural analyses were carried out with the monochromatic Cu-Kα radiation in the parallel beam geometry using RINT2000 (Rigaku) equipped with a W/Si multilayer mirror. The unit was operated at 50 kV and 30mA in a scanning step of 0.02^o and a scanning speed of 0.4^o/min. A JADE (Materials Data, Inc.) software equipped with Pearson-VII function was used to separate the α and ω peaks as well as to measure the area surrounded by each peak. For TEM observations, the 3mm discs used for the XRD analysis were ground mechanically to a thickness of 0.15mmand further thinned with a twin-jet electrochemical polisher using a solution of 10% $HClO_4$ and 90%

CH_3COOH at 25 ^oC. TEM was performed at 200 kV for microstructural observation and for recording selected-area electron diffraction (SAED) patterns. For DSC analysis, rectangular samples having dimensions of 3 mm × 2.7 mm were cut from the HPT-processed discs at 3 mm off-axis positions from the center. These samples were ground mechanically and thereafter cut to small pieces with widths less than 1mm. Such pieces with a totalweight of 40 mg were subjected to DSC in a heating rate of 5 ^oC/min.

3. Results and discussions

The hardness variations are shown in Fig. 2 with the equivalent strain at two different pressures of 2 and 6 GPa. For the applied pressure of 6 GPa, the microhardness increases with increasing equivalent strain at early stages of straining but saturates to a constant level where the hardness remains unchanged with further straining. This hardness behavior of Zr is similar to the behavior of pure Cu [22,23] and Fe [20]. However, unlike the pure Cu and Fe where the hardness level at the saturation is independent of the applied pressure [24], it is different in Zr depending on the applied pressure: 265 Hv at 2 GPa and 380 Hv at 6 GPa. The dependence on the pressure is more clearly documented in Fig. 3 covering a wide range of the pressure from 1 to 40 GPa. The saturation hardness increases abruptly at a pressure of ~4 GPa but slightly increases or remains essentially constant for the pressure range above ~6 GPa.

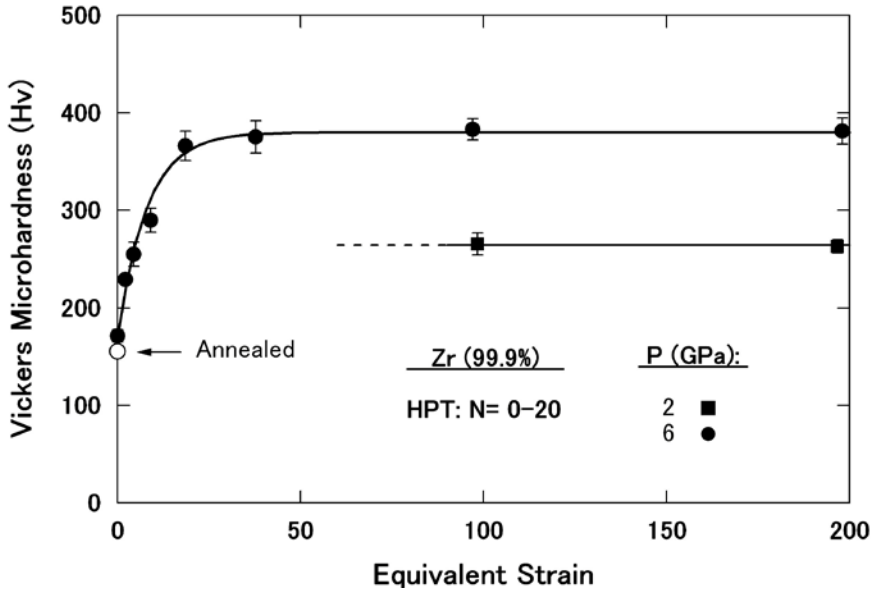

Fig. 2. Vickers microhardness plotted against equivalent strain for annealed sample and samples processed under pressures of 2 and 6 GPa for various revolutions.

The stress–strain curves are delineated in Fig. 4 for HPT samples after 10 revolutions under pressures of 2 and 6 GPa including an annealed sample. The tensile strength increases in consistence with the hardness measurement shown in Fig. 2. However, the total elongation to failure decreases with an increase in the pressure. Although the ductility of more than 10% is still

retained for the sample after processing with 2 GPa, the specimen failed with little ductility for the specimen processed with 6 GPa.

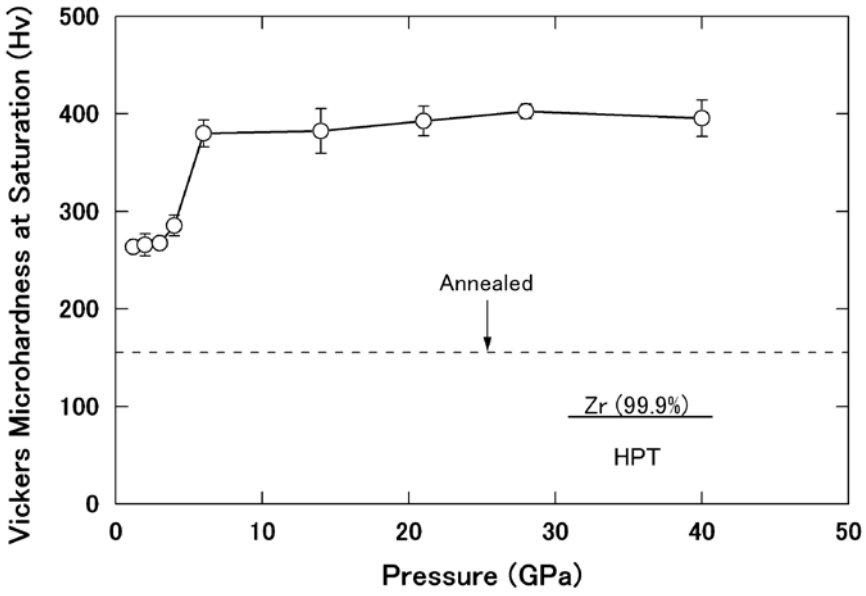

Fig. 3. Vickers microhardness at saturation plotted against applied pressure.

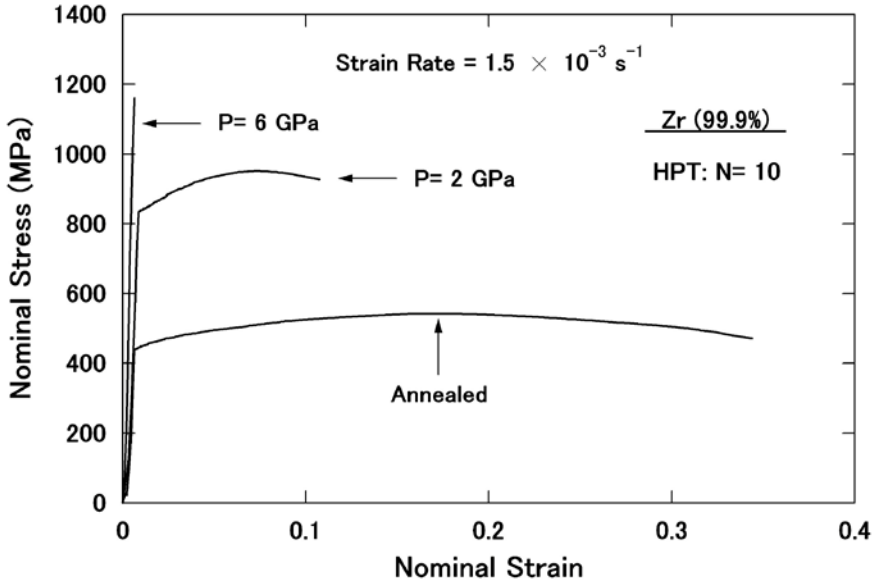

Fig. 4. Nominal stress versus nominal strain curves obtained for annealed sample and HPT discs processed for 10 revolutions under pressures of 2 and 6 GPa.

It is known that pure Zr transforms from α to ω phase in a Martensitic manner at pressures higher than 2 GPa [14–16,25]. This study has also confirmed the same phase transformation using XRD analysis. As shown in Fig. 5(a), the peak for the ω phase clearly appears at the pressure of 6 GPa. Since the ω phase is known as harder than the α phase [15,26], the formation of the ω phase at 6 GPa should be responsible for the increase in hardness at the saturation level as shown in Figs. 2 and 3 and with the increase in the tensile strength as shown in Fig. 4. The reduced ductility after

processing at 6 GPa as shown in Fig. 4 can be attributed to the presence of ω phase because it is brittle when compared with the α phase [15]. Close examination of Fig. 5(a) indicates the following three important points:

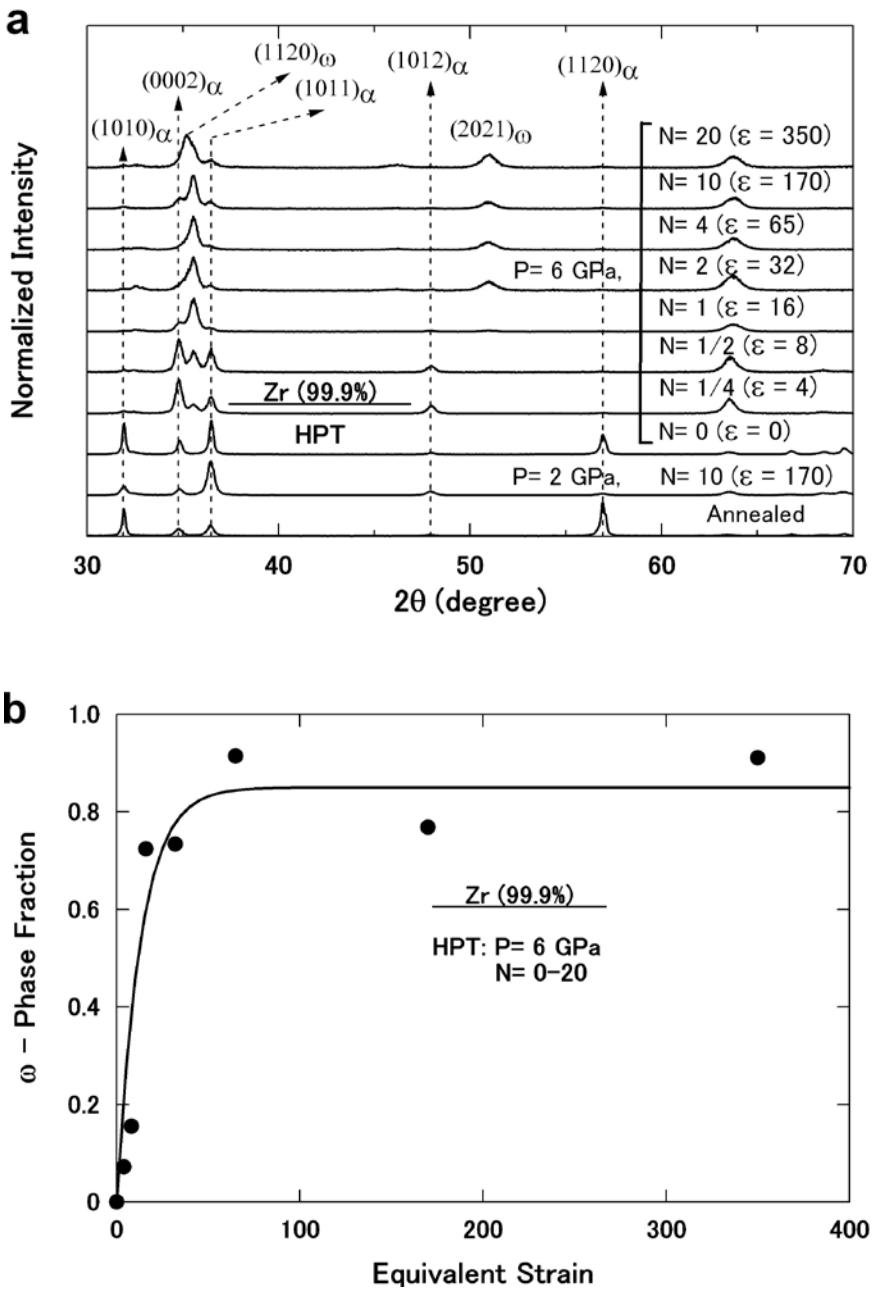

Fig. 5. (a) XRD profiles of Zr processed at 2 GPa for N = 10 and at 6 GPa for N = 1/4–20 including annealed sample and (b) fraction of ω phase plotted against equivalent strain.

(1) No visible peak is detected for the ω phase after the application of the pressure of 6 GPa but without rotation (N = 0). However, a peak for the ω phase clearly appears after rotation by N = 1/4 and the peak height increases with further revolution. Thus, the straining is effective for the α→ω phase transformation as well as for increasing the stability of ω phase after releasing the pressure in consistence with reports for Ti [17–19] and earlier reports for Zr [10,17].

(2) The peak intensities of $(10\bar{1}0)_\alpha$ and$(11\bar{2}0)_\alpha$ which are prominent in the annealed sample almost disappear after HPT for N = 1/4 at 6 GPa. They are also significantly reduced after HPT for N = 10 at 2 GPa but instead the peak of $(10\bar{1}1)_\alpha$ is increased under this pressure. This indicates that a texture may develop such that the basal plane of the α phase tends to be parallel to the disc surface by simultaneous rotation and compression.

(3) The intensity of $(11\bar{2}0)_\omega$ and $(20\bar{2}1)_\omega$ peaks increases with an increase in the strain but the relative intensity of $(11\bar{2}0)_\omega$ peak to $(20\bar{2}1)_\omega$ peak decreases with straining. It can be concluded that the ω phase initially forms with *c*-axis parallel to the pressing direction but as the strain increases *c*-axis trend to be perpendicular to the pressing direction.

Fig. 5(b) plots a change in the fraction of ω phase as a function of equivalent strain. Here, the ω phase fraction was calculated by taking ratio of the area surrounded by all ω phase peaks to the total area including the α and ω peaks. It is apparent that the fraction of the ω phase increases with the strain and remains constant at high strains more than ~50. This trend is very similar to the hardness variation with equivalent strain as shown in Fig. 2. However, the ω phase fraction reaches a level slightly less than 100%. Although this suggests that the complete transformation does not occur, there can be a possibility that a reverse transformation from the ω phase to the α phase might have occurred during mechanical polishing for the preparation of the XRD specimens as reported in an earlier experiment that the reverse transformation occurred during cold machining [15].

Therefore, the hardness saturation occurs in Zr not only because the hardening by straining is balanced by the softening by recovery and/or recrystallization as described for pure Cu [22,23] and Fe [20] but also there should be a balance between the formation and destruction of the ω phase during processing.

The lattice parameters (*a* and *c*) and the *c*/*a* ratio obtained by XRD measurements are given in Table 1. It is found that *a* and *c* for the α phase are almost the same for the annealed sample and the HPT-processed sample at 2 GPa and the lattice parameters are in good agreement with an earlier report [27]. However, a slight expansion of *a*-axis (~0.6%) for the α phase takes place due to the presence of ω phase at 6 GPa. For the ω phase, the lattice parameter of *a*-axis is in good agreement with the earlier reports [28,29] but there is a slight reduction in *c*-axis (~1%) as shown in Table 1.

Table 1. Lattice parameters (*a*, *c* and *c*/*a*) for α and ω phases of Zr after annealing and after HPT processing at 2 and 6 GPa for *N*= 10 revolutions in comparison with the published data [27–29].

	α phase				ω phase		
	Annealed	HPT, P= 2 GPa, N = 10	HPT, P= 6 GPa, N = 10	Ref. [27]	HPT, P= 6 GPa, N = 10	Ref. [28]	Ref. [29]
c (nm)	0.5164	0.5161	0.5190	0.5148	0.3091	0.3109	0.3136
a (nm)	0.3233	0.3233	0.3236	0.3231	0.5053	0.5036	0.5039
c/*a*	1.597	1.596	1.603	1.593	0.612	0.617	0.622

TEM microstructures and the corresponding SAED patterns were shown in Fig. 6 for samples after 10 revolutions under pressures of (a) 2 GPa and (b) 6 GPa. It should be noted that both conditions correspond to the saturation level where no change in hardness occurs with straining. It

is apparent from Fig. 6(a) that the microstructure consists of small grains with an average grain size of ~200 nm for the pressure of 2 GPa but the grain size appears to decrease to ~100 nm for the pressure of 6 GPa in Fig. 6(b). The grain sizes at both conditions were obtained by recording several dark-field images and by measuring two orthogonal axes of the bright areas corresponding to individual grains. Close observation of the microstructures reveals that there are many dislocations within the grains and most of the grains are surrounded by ill-defined grain boundaries. Whereas some dislocation-free grains were observed in earlier reports for pure Cu [22] and pure Fe [20], such grains are rarely seen in this study for Zr. The significant grain refinement under both pressures was achieved by introduction of intense strain as reported in other metals and alloys [20,22] but the finer grain size under 6 GPa can be attributed to the ω phase formation as presented above. The presence of the remaining α phase in the ω phase matrix might have acted as inhibitors for grain boundary movement. It should be noted, therefore, that the additional increase in the hardness at the pressures more than 4 GPa shown in Figs. 2 and 3 must be due to the finer grain size as well as the harder ω phase formation.

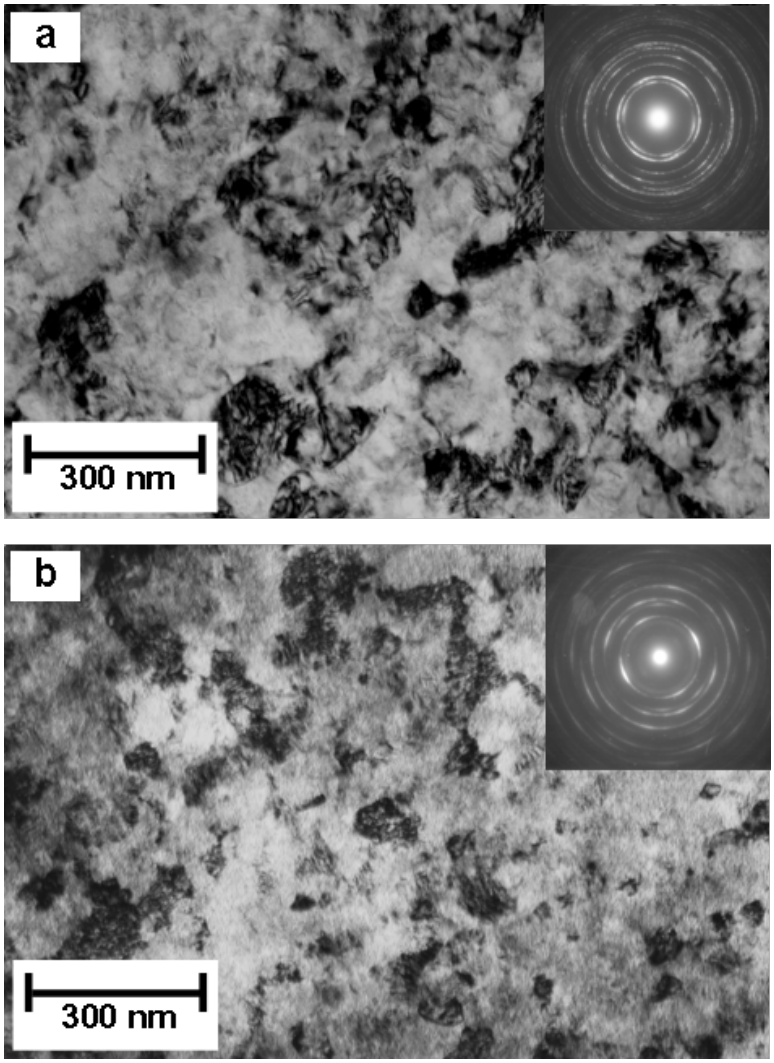

Fig. 6. TEM bright-field micrographs and SAED patterns for samples processed under pressures of: (a) 2 GPa and (b) 6 GPa after revolutions of $N = 10$.

The variation of heat flow with temperature after DSC analysis of the annealed sample and the HPT-processed samples is shown in Fig. 7(a). No peak is visible for the annealed sample and the HPT-processed sample at 2 GPa because there is no phase transformation in these samples. No peak is seen for the ω→α phase transformation despite the fact that the XRD analysis led to the presence of 15% of the ω phase after HPT under 6 GPa for N = 1/2. One additional DSC analysis was carried out with the sample processed under the same HPT condition but subjected to electro-chemical polishing. Nevertheless, no ω peak was detected and thus, the discrepancy between the XRD and DSC results for this sample should be because of a lower sensitivity of DSC in comparison with the XRD. However, a peak for ω→α phase transformation appears after processing at 6 GPa for the revolutions larger than 1/2 and it shifts to higher temperature as the imposed strain increases.

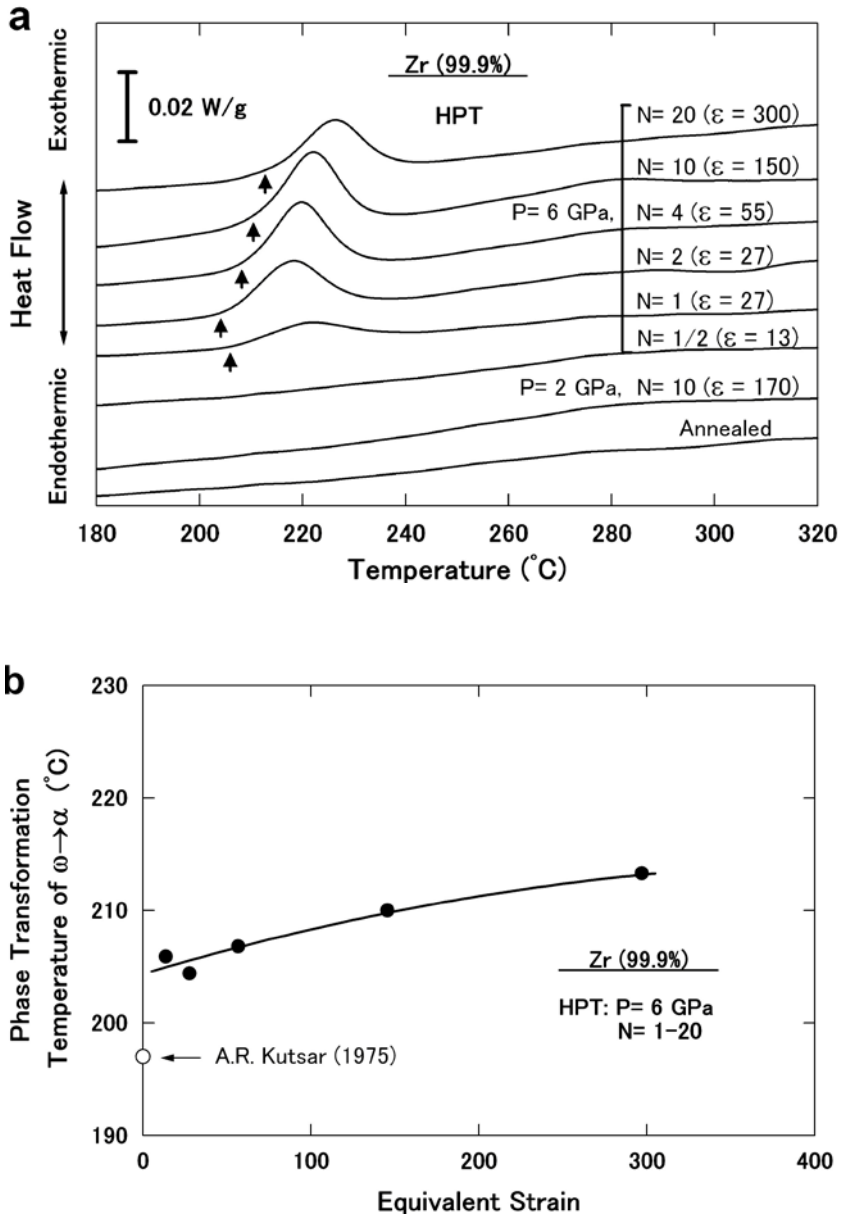

Fig. 7. (a) DSC curves of Zr processed at 2 GPa for N = 10 and at 6 GPa for N = 1/2–20 including annealed sample and (b) temperature of ω→α phase transformation plotted against equivalent strain. Arrows in (a) indicate onsets of heat flow.

The increase in the transformation temperature with strain is more clearly demonstrated in Fig. 7(b) where the temperatures for the onset of heat flow as indicated by arrows in Fig. 7(a) are plotted as a function of equivalent strain. In Fig. 7(b), the transformation temperature, 195 ^{o}C, obtained by Kutsar [14] is also included and it is lower by 10 ^{o}C than the transformation temperatures obtained in this study. For this difference, it is most conceivable that the sample in this study contains large strain which makes the ω phase stable to retain at higher temperature. As given in Table 1, there are large differences in the lattice constants between the α phase and the ω phase and this can result in increasing the critical energy for the reverse ω→α phase transformation as argued by Estrin [30] and Vohra [31]. Thus, it is anticipated that the temperature for the reverse transformation is increased with increasing the imposed strain. In fact the relative orientation and stability of ω phase with respect to the α phase changes with straining as found from Fig. 5(a) even at the strains higher than ~50. It should be noted that the ω phase obtained in this study is stable for at least 400 days at 25 ^{o}C and its fraction remains unchanged for this period of time. Thus, straining can increase not only the fraction of ω phase but also the thermal stability.

4. Summary and conclusions

High-pressure torsion (HPT) was conducted on pure Zr (99.9%) at applied pressures up to 40 GPa and the following conclusions were obtained.

(1) Vickers microhardness measurements revealed that the hardness increases with an increase in the equivalent strain at early stages of straining and saturates into a steady state level at an equivalent strain of ~50. The hardness level at the steady state is almost constant at pressures up to 4 GPa and increases abruptly at a pressure range of 4–6 GPa but slightly increases or remains essentially constant for the pressure range above ~6 GPa.

(2) Tensile testing showed that an increase in the applied pressure from 2 to 6 GPa results in an increase in UTS from 950 to 1150 MPa and a decrease in ductility from 10% to zero.

(3) TEM observation showed that the average grain size at the steady state for the pressures of 2 and 6 GPa is ~200 and ~100 nm, respectively.

(4) XRD analysis revealed that the increase in hardness and strength and the decrease in ductility and grain size at the saturation for HPT-processed samples at 6 GPa are due to the α→ω phase transformation. The ω phase initially forms with *c*-axis parallel to the pressing direction but as the strain increases, the *c*-axis tends to be perpendicular to the pressing direction. XRD analysis also suggested that the *c*-axis for α phase is expanded about ~0.6% in the presence of ω phase.

(5) DSC analysis showed that the temperature for the reverse transformation from ω to α phase increases with straining.

(6) The ω phase obtained by HPT processing of Zr in this study was stable for at least 400 days at room temperature.

Acknowledgements

One of the authors (KE) would like to thank the Islamic Development Bank for a scholarship. This work was supported in part by a Grant-in-Aid for Scientific Research from the

Ministry of Education, Culture, Sports, Science and Technology, Japan, in Priority Areas “Giant Straining Process for Advanced Materials Containing Ultra-High Density Lattice Defects” and in part by Kyushu University Interdisciplinary Programs in Education and Projects in Research Development (P&P).

References

[1] R.Z. Valiev, R.K. Islamgaliev, I.V. Alexandrov, Prog. Mater. Sci. 45 (2000) 103–189.

[2] R.Z. Valiev, I.V. Alexandrov, Y.T. Zhu, T.C. Lowe, J. Mater. Res. 17 (2002) 5–8.

[3] A.P. Zhilyaev, T.G. Langdon, Prog. Mater. Sci. 53 (2008) 893–979.

[4] S.H. Yu, H.S. Ryoo, D.H. Shin, S.K. Hwang, MRS Symposium Proceedings 730, 1999, pp. 143–148.

[5] W.S. Choi, H.S. Ryoo, S.K. Hwang, M.H. Kim, S.I. Kwun, S.W. Chae, Metall. Mater. Trans. A 22 (2002) 973–980.

[6] S.H. Yu, Y.B. Chun, S.K. Hwang, D.H. Shin, Philos. Mag. 85 (2005) 345–371.

[7] B.K. Kad, J.M. Gebert, M.T. Perez-Prado, M.E. Kassner, M.A. Meyers, Acta Mater. 54 (2006) 4111–4127.

[8] L. Saldana, A. Mendez-Vilas, L. Jiang, M. Multigner, J.L. Gonzalez-Carrasco, M.T. Perez-Prado, M.L. Gonzalez-Martın, L. Munuera, N. Vilaboa, Biomaterials 28 (2007) 4343–4354.

[9] L. Jiang, O.A. Ruano, M.E. Kassner, M.T. Perez-Prado, JOM 59 (6) (2007) 42–45.

[10] M.T. Perez-Prado, A.A. Gimazov, O.A. Ruano, M.E. Kassnerc, A.P. Zhilyaev, Scripta Mater. 58 (2008) 219–222.

[11] L. Jiang, M.T. Perez-Prado, P.A. Gruber, E. Arzt, O.A. Ruano, M.E. Kassner, Acta Mater. 56 (2008) 1228–1242.

[12] G.P. Dinda, H. Rosner, G.Wilde, Scripta Mater. 52 (2005) 577–582.

[13] Y.K. Vohra, S.K. Sikka, S.N. Vaidya, R. Chidamberan, J. Phys. Chem. Solids 38 (1977) 1293–1296.

[14] A.R. Kutsar, Fiz. Metal. Metalloved. 40 (1975) 786–793.

[15] S.K. Sikka, Y.K. Vohra, R. Chidambaram, Prog. Mater. Sci. 27 (1982) 245–310.

[16] D. Errandonea, Y. Meng, M. Somayazulu, D. Haussermann, Physica B 355 (2005) 116–125.

[17] V.A. Zilbershtein, N.P. Chistotina, A.A. Zharov,N.S. Grishina, E.I. Estrin, Fiz.Metal. Metalloved. 39 (1975) 445–447.

[18] A.R. Kilmametov, A.V. Khristoforova, G. Wilde, R.Z. Valiev, Z. Kristallogr. Suppl. 26 (2007) 339–344.

[19] Y. Todaka, J. Sasaki, T. Moto, M. Umemoto, Scripta Mater. 59 (2008) 615–618.

[20] K. Edalati, T. Fujioka, Z. Horita, Mater. Trans. 50 (2008) 44–50.

[21] K. Edalati, Z. Horita, T.G. Landgon, Scripta Mater. 60 (2009) 9–12.

[22] K. Edalati, T. Fujioka, Z. Horita, Mater. Sci. Eng. A 497 (2008) 168–173.

[23] Y. Ito, Y. Harai, T. Fujioka, K. Edalati, Z. Horita, Mater. Sci. Forum. 548–586 (2008) 191–196.

[24] K. Edalati, T. Fujioka, Z. Horita, Proceedings of 156th Meeting of ISIJ and JIM: Joint SessiononCurrentAdvances inMaterials and Processes,Kumamoto, Japan, 21(2), 2008, p. 516.
[25] M.P. Usikov, V.A. Zilbershtein, Phys. Status Solidi 19a (1973) 53–58.
[26] F.R. Brotzen, E.L. Harmon, A.R. Troiano, J. Met. 7 (1955) 413–419.
[27] B.D. Cullity, Elements of X-ray Diffraction, second ed., Addison-Wesley, Reading, MA, 1977.
[28] J.C. Jameson, Science 140 (1963) 72.
[29] B. Olinger, J.C. Jamieson, High Temp.–High Pressures 5 (1973) 123–135.
[30] E.I. Estrin, Fiz. Metal. Metalloved. 37 (1974) 1249–1255.
[31] Y.K. Vohra, J. Nucl. Mater. 7.5 (1978) 288–293.